

Dear Author,

Here are the proofs of your article.

- You can submit your corrections **online**, via **e-mail** or by **fax**.
- For **online** submission please insert your corrections in the online correction form. Always indicate the line number to which the correction refers.
- You can also insert your corrections in the proof PDF and **email** the annotated PDF.
- For fax submission, please ensure that your corrections are clearly legible. Use a fine black pen and write the correction in the margin, not too close to the edge of the page.
- Remember to note the **journal title**, **article number**, and **your name** when sending your response via e-mail or fax.
- **Check** the metadata sheet to make sure that the header information, especially author names and the corresponding affiliations are correctly shown.
- **Check** the questions that may have arisen during copy editing and insert your answers/ corrections.
- **Check** that the text is complete and that all figures, tables and their legends are included. Also check the accuracy of special characters, equations, and electronic supplementary material if applicable. If necessary refer to the *Edited manuscript*.
- The publication of inaccurate data such as dosages and units can have serious consequences. Please take particular care that all such details are correct.
- Please **do not** make changes that involve only matters of style. We have generally introduced forms that follow the journal's style. Substantial changes in content, e.g., new results, corrected values, title and authorship are not allowed without the approval of the responsible editor. In such a case, please contact the Editorial Office and return his/her consent together with the proof.
- If we do not receive your corrections **within 48 hours**, we will send you a reminder.
- Your article will be published **Online First** approximately one week after receipt of your corrected proofs. This is the **official first publication** citable with the DOI. **Further changes are, therefore, not possible.**
- The **printed version** will follow in a forthcoming issue.

Please note

After online publication, subscribers (personal/institutional) to this journal will have access to the complete article via the DOI using the URL: [http://dx.doi.org/\[DOI\]](http://dx.doi.org/[DOI]).

If you would like to know when your article has been published online, take advantage of our free alert service. For registration and further information go to: <http://www.link.springer.com>.

Due to the electronic nature of the procedure, the manuscript and the original figures will only be returned to you on special request. When you return your corrections, please inform us if you would like to have these documents returned.

Metadata of the article that will be visualized in OnlineFirst

ArticleTitle	Thermo-migration behavior of SAC305 lead-free solder reinforced with fullerene nanoparticles	
Article Sub-Title		
Article CopyRight	Springer Science+Business Media New York (This will be the copyright line in the final PDF)	
Journal Name	Journal of Materials Science	
Corresponding Author	Family Name	Liu
	Particle	
	Given Name	Changqing
	Suffix	
	Division	Wolfson School of Mechanical
	Organization	Electrical and Manufacturing Engineering, Loughborough University
	Address	Loughborough, UK
	Email	C.Liu@lboro.ac.uk
	ORCID	
Corresponding Author	Family Name	Wu
	Particle	
	Given Name	Fengshun
	Suffix	
	Division	State Key Laboratory of Materials Processing and Die and Mould Technology
	Organization	Huazhong University of Science and Technology
	Address	Wuhan, 430074, China
	Email	fengshunwu@hust.edu.cn
	ORCID	
Author	Family Name	Chen
	Particle	
	Given Name	Guang
	Suffix	
	Division	State Key Laboratory of Materials Processing and Die and Mould Technology
	Organization	Huazhong University of Science and Technology
	Address	Wuhan, 430074, China
	Division	Wolfson School of Mechanical
	Organization	Electrical and Manufacturing Engineering, Loughborough University
	Address	Loughborough, UK
	Email	
	ORCID	
Author	Family Name	Liu
	Particle	
	Given Name	Li
	Suffix	

Division Wolfson School of Mechanical
Organization Electrical and Manufacturing Engineering, Loughborough University
Address Loughborough, UK
Email
ORCID

Author Family Name **Du**
Particle
Given Name **Juan**
Suffix
Division Wolfson School of Mechanical
Organization Electrical and Manufacturing Engineering, Loughborough University
Address Loughborough, UK
Email
ORCID

Author Family Name **Silberschmidt**
Particle
Given Name **Vadim V.**
Suffix
Division Wolfson School of Mechanical
Organization Electrical and Manufacturing Engineering, Loughborough University
Address Loughborough, UK
Email
ORCID

Author Family Name **Chan**
Particle
Given Name **Y. C.**
Suffix
Division Department of Electronic Engineering
Organization City University of Hong Kong
Address Tat Chee Avenue, Kowloon Tong, Hong Kong
Email
ORCID

Schedule Received 18 April 2016
Revised
Accepted 18 July 2016

Abstract In this work, SAC305 lead-free solder reinforced with 0.1 wt. % fullerene nanoparticles was prepared using a powder metallurgy method. A lab-made setup and a corresponding Cu/solder/Cu sample for thermo-migration (TM) test were designed and implemented. The feasibility of this setup for TM stressing was further verified with experimental and simulation methods; a temperature gradient in a solder seam was calculated as 1070 K/cm. Microstructural evolution and mechanical properties of both plain and composite solder alloys were then studied under the condition of TM stressing. It was shown that compared to unreinforced SAC305 solder, the process of diffusion of Cu atoms in the composite solder seam was remarkably suppressed. After the TM test for 600 h, Cu/solder interfaces in the composite solder seam were more stable and the inner structure remained more intact. Moreover, the addition of fullerene reinforcement can considerably affect a distribution of Cu_6Sn_5 formed as a result of dissolution of Cu atoms during the TM test. Hardness data across the solder seam were also found notably different because of the elemental redistribution caused by TM.

_2D materials	_EBSD	_materials design	_resorbable materials
_ab initio calculations	_elastic properties	_materials for demanding environments	_responsive materials
_additive manufacturing	_electrical properties	_materials for energy	_rheology
_adhesion	_electrocatalysis	_mechanical properties	_sapphire/Al ₂ O ₃
_adsorption	_electrochemistry	_membranes	_scaffolds
_aerogels	_electrode materials	_mesoporous materials	_scanned-probe microscopy
_AFM	_electron-beam melting	_metal-insulator transition	_selective laser melting
_alloys	_electronic materials	_metal/organic frameworks (MOFs)	_self-assembly
_amorphous materials	_electronic properties	_metallic glasses	_self-healing materials
_annealing	_electrospinning	_metals	_SEM
_antifouling materials	_embrittlement	_metamaterials	_semiconductors
_atomic-layer deposition (ALD)	_energy harvesting	_microanalysis	_sensing and sensors
_atomistic modeling	_epitactic or epitaxial growth	_microstructure	_severe plastic deformation
_batteries	_fatigue	_minerals or mineralization	_shape memory materials
_batteries, lithium	_FCC metals	_molding	_silicones
_batteries, magnesium	_ferroelectrics	_molecular dynamics	_singlet-exciton fission
_batteries, sodium	_FGMs	_molecular simulation	_sintering
_BCC metals	_fibers or fiber technology	_molecular-beam epitaxy (MBE)	_small volume testing
_bio-inspired materials	_food colloids	_morphology	_smart materials
_biomass conversion	_fracture	_multiferroics	_sodium-sulphur batteries
_biomaterials	_fuel cells	_multilayers	_soft interfaces
_biomechanics	_functional anisotropy	_nanocomposites	_soft matter
_biomimetic	_functional materials	_nanofunctionality	_sol-gel preparation
_black phosphorus	_gas-phase transport	_nanoindentation	_solidification
_blends	_gelation	_nanolithography	_solvothermal/hydrothermal
_brazing	_geocomposites	_nanomaterials	_spectroscopy (XPS)
_calcification	_glass	_nanomedicines	_spin glass
_capacitors	_grain boundaries	_nanoporous materials	_spintronics
_carbon fiber	_grain boundary engineering	_natural materials	_sputter deposition
_carbon nanotube	_graphene	_NDT	_STM
_casting	_graphitic carbon	_NMR	_superalloys
_catalysts or catalysis	_hardness	_nuclear materials	_supercapacitors
_cellular materials	_HCP metals	_nucleation	_superconductors
_cellulose	_healing	_omniphobic materials	_superelasticity
_ceramics	_heat treatment	_optical materials and properties	_superhydrophobic
_characterization methods	_hierarchical materials	_organic electronics	_surface treatments
_chemical vapor deposition (CVD)	_high entropy alloys	_organic solar-cell materials	_surfaces
_CO ₂ sequestration	_high pressure torsion	_permeable materials	_surfactants
_coatings	_high throughput testing	_perovskite	_technical textiles
_colloids or bio-colloids	_hot isostatic pressing	_perovskite solar cell (PSCs)	_TEM
_composite materials	_hydrogels	_phase diagrams	_texture
_computational materials science	_hydrogen storage or production	_phase transformations	_theranostics
_computer modeling	_hydrolysis	_phase-change materials (PCMs)	_thermal barrier coatings
_computer simulation	_II-VI compounds	_phase-field modeling	_thermal properties
_conducting polymers	_III-V compounds	_phosphors	_thermodynamics
_corrosion and oxidation	_imaging	_photocatalysis	_thermoelectrics
_corrosion protection	_In situ or operando	_photonic materials	_thin-film or thick-film coatings
_crystal plasticity	_infrared spectroscopy	_photoreactive materials	_TiO ₂ rutile, anatase or brookite
_crystallization	_intercalation	_phototherapeutics	_tissue engineering
_curing	_interfaces	_photovoltaics (solar cells)	_tomography
_data analytics	_intermetallics	_piezoelectric materials	_topological insulators
_defects	_ionomers	_plasma deposition	_transparent conductors
_deformation	_kinetics	_plasmonic materials	_transport mechanisms
_deposition	_laminates	_plating	_tribology
_dielectrics	_laser processing	_polymers	_twinning
_diffraction, electron	_latticed effects	_porous materials	_TWIP steels
_diffraction, neutron	_layered materials	_powder technology	_two-photon adsorption
_diffraction, X-ray (XRD)	_light alloys	_pyroelectrics	_UFG materials
_diffusion	_light-emitting diodes	_quasicrystals	_viscoelasticity
_diodes	_liquid crystals	_radiation damage	_viscosity
_dislocation dynamics	_lithography	_radiation effects	_water-splitting
_dislocations	_machining	_rapidly solidified materials	_wear
_drug delivery	_macro defects	_redox flow batteries	_wood
_dye-sensitized solar cells (DSSCs)	_magnetic materials or properties	_regenerative medicine	_XPS
_dysfunctional materials	_magnetic ordering		_zeolite

Thermo-migration behavior of SAC305 lead-free solder reinforced with fullerene nanoparticles

Guang Chen^{1,2}, Li Liu², Juan Du², Vadim V. Silberschmidt², Y. C. Chan³, Changqing Liu^{2,*}, and Fengshun Wu^{1,*}

¹ State Key Laboratory of Materials Processing and Die and Mould Technology, Huazhong University of Science and Technology, Wuhan 430074, China

² Wolfson School of Mechanical, Electrical and Manufacturing Engineering, Loughborough University, Loughborough, UK

³ Department of Electronic Engineering, City University of Hong Kong, Tat Chee Avenue, Kowloon Tong, Hong Kong

Received: 18 April 2016

Accepted: 18 July 2016

© Springer Science+Business Media New York 2016

ABSTRACT

In this work, SAC305 lead-free solder reinforced with 0.1 wt. % fullerene nanoparticles was prepared using a powder metallurgy method. A lab-made setup and a corresponding Cu/solder/Cu sample for thermo-migration (TM) test were designed and implemented. The feasibility of this setup for TM stressing was further verified with experimental and simulation methods; a temperature gradient in a solder seam was calculated as 1070 K/cm. Microstructural evolution and mechanical properties of both plain and composite solder alloys were then studied under the condition of TM stressing. It was shown that compared to unreinforced SAC305 solder, the process of diffusion of Cu atoms in the composite solder seam was remarkably suppressed. After the TM test for 600 h, Cu/solder interfaces in the composite solder seam were more stable and the inner structure remained more intact. Moreover, the addition of fullerene reinforcement can considerably affect a distribution of Cu₆Sn₅ formed as a result of dissolution of Cu atoms during the TM test. Hardness data across the solder seam were also found notably different because of the elemental redistribution caused by TM.

Introduction

SAC305 (wt. %) lead-free solder is widely used in electronic interconnections, thanks to its outstanding mechanical properties and good reliability under service conditions [1–3]. However, with fast developments in miniaturization and integration density in high-density electronic packages, electro- and thermo-

migration (TM) failures induced by a high current density and large thermal gradients have become a main problem which would threaten the reliability of SAC305 solder interconnections [4–8]. The microstructural and mechanical evolution together with failure modes of solder joints under TM and EM stressing were also reported in previous studies [9–14]. Abdulhamid et al. [9] comprehensively

Address correspondence to E-mail: C.Liu@lboro.ac.uk; fengshunwu@hust.edu.cn

54 investigated the damage mechanics of 95.5Sn4Ag
55 0.5Cu (SAC405) lead-free solder joints under TM
56 stressing. After 1156 h TM stressing, they found that
57 the Cu concentration in cold side is significantly
58 higher than in hot side, while vacancy migration and
59 Sn grain coarsening are in the opposing direction. In
60 order to deeply understand the TM process, a fully
61 coupled thermo-mechanical model is introduced by
62 Basaran et al. [10]; the TM induced strength degra-
63 dation and grain coarsening effects were both ana-
64 lyzed. Further, they also comparatively studied the
65 migration mechanism in solder joints under EM and
66 EM/TM stressing [12]. It was also reported that TM is
67 more likely to lead to failures of solder joints in some
68 cases [15]. Therefore, with the trend of decreasing
69 interconnection height, lead-free solder interconnec-
70 tions will face with reliability challenges related to
71 electro-migration (EM) and in particular, TM.

72 According to previous studies, mechanical prop-
73 erties and solderability of existing lead-free solders
74 could be improved by adding some foreign rein-
75 forcement (including metals, ceramics, and carbon-
76 based materials) into a solder matrix to prepare a
77 composite solder [16–21]. In addition, some
78 researchers also attempted to investigate an effect of
79 foreign reinforcement on EM in solder joints; it was
80 reported that a suitable type and an appropriate
81 amount of reinforcement added showed a positive
82 effect on suppressing EM in solder joints [22–27].
83 However, to date, a systematic study of TM behavior
84 of composite solder interconnections containing for-
85 eign reinforcement under large temperature gradient
86 is still lacking.

87 As a zero-dimensional carbon-based nanomaterial,
88 a unique molecular structure of fullerene determines
89 its physical stability, low density as well as its
90 excellent electrical, thermal, and mechanical proper-
91 ties [28–32]. Hence, it was usually used as reinforcing
92 phase in preparing polymer- and metal-based com-
93 posite materials [33, 34]. Chernogorova et al. [33]
94 reported that tensile strength and microhardness of
95 an aluminum/C60 composite alloy were significantly
96 improved with the addition of C60 reinforcement.
97 Watanabe et al. [34] fabricated an Mg–Al–Zn/fuller-
98 ene (C60) composite alloy with a powder metallurgy
99 method; the produced material demonstrated super-
100 elasticity under 548 K (with 256 % elongation). Our
101 research group also prepared a SAC305/fullerene
102 (mixture of C60 and C70) composite solder with a
103 powder metallurgy method; the influence of fullerene

on microstructure and mechanical properties on SAC 104
solder joints were also systematically studied. It was 105
found that addition of a proper amount of fullerene 106
was effective in microstructural refinement and 107
improvement in mechanical properties of solder 108
joints [35]. To study further the effect of fullerene 109
reinforcement on thermo-migration behavior of sol- 110
der joints, in this paper, a SAC/fullerene composite 111
solder reinforced with nano-sized fullerene particles 112
was similarly prepared with the powder metallurgy 113
method. Cu/Solder/Cu-structured interconnections 114
were then formed for subsequent thermo-migration 115
tests. It is widely reported that TM in Sn-based solder 116
joints can be triggered when a temperature gradient 117
and an environmental temperature reach at least 118
1000 K/cm and 100 °C, respectively [36]. Therefore, 119
for TM tests, to achieve a large enough thermal gra- 120
dient and environmental temperature without 121
involving EM factor, a TM setup based on a heating 122
plate with constant temperature and a Peltier ther- 123
moelectric cooler was designed and prepared. Feasi- 124
bility of the as-designed setup and corresponding 125
samples was also further verified in this work. 126

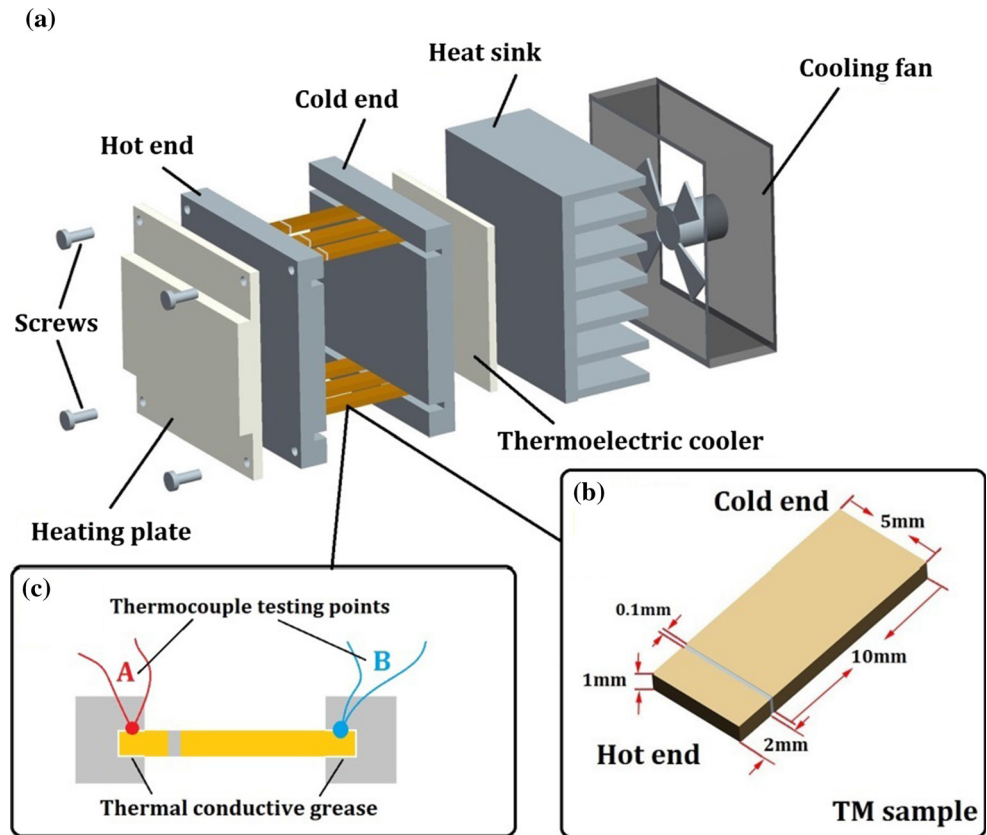
127 After progressively prolonged TM tests, evolution 127
of interfacial intermetallics (IMCs) at the hot and cold 128
ends and microstructure at the center of both plain 129
and composite solder seams were comparatively 130
studied. Additionally, the dissolution of Cu atoms 131
into the solder seams was quantitatively evaluated. 132
Moreover, the change in mechanical properties of the 133
solder seams as a result of redistribution of elements 134
during the TM test was also investigated. The find- 135
ings in this work could promote our understanding 136
of the impact of thermal gradient and environmental 137
temperature on reliability of composite solder joints 138
without the effect of current. It can also facilitate 139
future studies on mitigating failures in solder joints 140
induced by thermo-migration. 141

142 Experimental

143 Preparation of composite solder

144 SAC305 (wt. %) lead-free solder powder (with
145 diameter of 25–45 μm, Beijing Compo, China) and a
146 mixture of fullerene nanoparticles (approximately
147 80 % C60 and 20 % C70 with an average diameter of
148 30 nm, JCNANO Materials Tech, China) were uti-
149 lized as original materials. For preparation of

Figure 1 Schematic diagram of TM setup (a), TM samples (b), and thermocouple positions (c).



150 composite solder, the preweighted solder powder
 151 (99.9 wt %) and fullerene particles (0.1 wt. %) were
 152 homogenously blended in a planetary ball mill for
 153 20 h. The mixed powder was then uniaxially com-
 154 pacted into solder billets (24 mm × 8 mm × 3 mm).
 155 These compacted solder billets were then sintered at
 156 180 °C for 3 h in a vacuum sintering furnace before
 157 rolling into solder foils (with thickness of 100 μm) to
 158 prepare TM samples.

159 Design and preparation of TM setup 160 and sample

161 To achieve a large enough thermal gradient across
 162 solder seams, a lab-made TM test setup was designed
 163 and prepared (as shown in Fig. 1a). The TM setup
 164 consisted of a constant-temperature heating plate
 165 with a temperature of 250 ± 5 °C as the heat resource
 166 and a Peltier thermoelectric cooler for cooling. A
 167 stable initial temperature (0 ± 2 °C) of the thermo-
 168 electric cooler was guaranteed by a temperature
 169 controller, while a heat sink and cooling fan were
 170 used to ensure its proper functioning during current
 171 stressing. The heating and cooling components were

172 fixed on corresponding Cu bases with grooves (they
 173 were also the hot and cold sides in the TM tests). The
 174 spacing between two Cu bases was kept as 10 mm,
 175 while rectangular grooves with depth of 1 mm
 176 for placing TM samples were also produced on both
 177 hot and cold Cu bases with wire-electrode cutting.
 178 According to the difference of coefficients of heat
 179 conduction for different materials, the sample for TM
 180 was designed as an asymmetrical structure with a
 181 shorter hot end (2 mm) and a longer cold end
 182 (10 mm); a Cu plate (with thickness of 1 mm and
 183 width of 5 mm) was used as substrate material for
 184 both hot and cold sides of the sample. For sample
 185 preparation, end surfaces of the Cu substrates of both
 186 sides were well polished before soldering. A solder
 187 foil with dimensions of 5 mm × 1 mm × 0.1 mm
 188 was then clamped between two Cu substrates; finally,
 189 the clamped Cu substrates and the solder foil to-
 190 gether with the clamp were placed in a reflow oven
 191 to prepare a sample of Cu/solder/Cu sandwich-like
 192 structure. The width of solder seams in reflowed
 193 solder samples remained similar to the thickness of
 194 the initial solder foils (namely, 100 μm); schematic
 195 diagram of a reflowed sample is shown in Fig. 1b. For

196 the TM tests, the hot and cold ends of the prepared
 197 sample were correspondingly embedded in the
 198 above-mentioned grooves on both hot and cold Cu
 199 bases; the embedded depth was approximately
 200 1 mm. To ensure good thermal conduction, thermal
 201 silicone grease was applied on each contact surface
 202 between different parts in the tests. In order to know
 203 the levels of temperature gradient and environmental
 204 temperature in the solder seam, experimental mea-
 205 surements and finite-element modeling were
 206 employed to evaluate the feasibility of the TM setup
 207 and the samples. A finite-element model was built
 208 with ANSYS 15.0 according to the actual dimensions
 209 of the setup and sample. To get good modeling
 210 results for a temperature distribution across the sol-
 211 der seam, thermocouples were first utilized to obtain
 212 the real temperature at points A and B during current
 213 stressing (the distances from A and B to the solder
 214 seam were 1 mm and 9 mm, respectively, as illus-
 215 trated in Fig. 1c). The obtained average temperatures
 216 for points A and B were recorded when the temper-
 217 ature difference reached a balance; the recorded data
 218 were then set as the loading temperatures of the two
 219 ends for the subsequent modeling.

220 TM tests and characterization

221 In the TM tests, five samples for each kind of solder
 222 (plain and composite) were tested to satisfy different
 223 testing purposes. Specifically, microstructural evolu-
 224 tion of one selected sample for each kind of solder
 225 was continuously observed a using scanning electron
 226 microscope (SEM QURTA 200) every 200 h; the total
 227 stressing time of the TM tests was designed as 600 h.
 228 The rest of samples that experienced the same TM
 229 stressing process were used for mechanical and
 230 compositional analysis. A focused ion beam (FIB)
 231 system was employed to study the distribution of Cu-
 232 Sn IMCs within a subsurface layer of the studied
 233 solder seams, while features of the inner structure
 234 were studied with an X-ray Micro-CT scanner (Metris
 235 XT H 160Xi) before and after the TM tests. Mechan-
 236 ical properties of the solder seams before and after
 237 the TM tests were also evaluated with a nanoindenter
 238 (Hysitron Ti750) at a constant load rate of 10 mN and
 239 a dwell time of 5 s. To know the difference in
 240 mechanical properties in different areas, in nanoin-
 241 dentation tests, each solder seam was evenly divided
 242 into three areas, denoted as A, B, and C at different
 243 positions between cold and hot ends. Five randomly

selected locations for each area were tested to ensure
 reliability of the test results. In addition, to evaluate
 quantitatively the process of dissolution of Cu atoms
 into the solder seams under a large temperature
 gradient, the seams were cut off from the TM samples
 after different TM stressing times. After that, residual
 Cu at the surface of the solder seams was removed by
 fine polishing. The treated solder seams were then
 ultrasonically dissolved in aqua regia solution for
 elemental analysis using an inductively coupled
 plasma optical emission spectroscopy (ICP-OES,
 Varian-720) with test precision at PPM level.

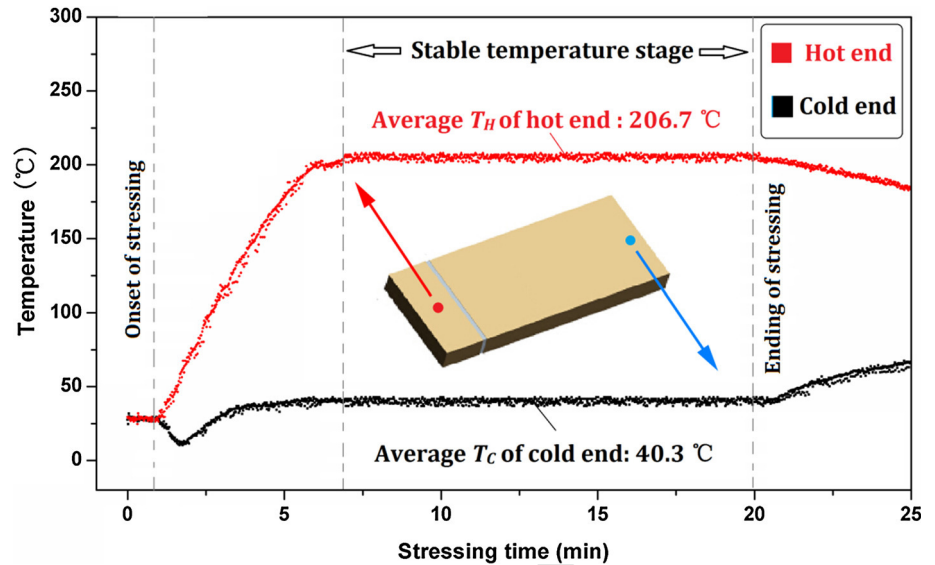
Results and discussion

Feasibility evaluation of TM setup and sample

Evolution of measured temperature at points A and B
 with the stressing time in the TM test is shown in
 Fig. 2. It can be seen from the curves that the tem-
 perature saw a continual increase at the hot end after
 current stressing, while the temperature of the cold
 end demonstrated a small decrease first and then
 increased gradually; after approximately 7 min of the
 stressing, the temperature difference between the hot
 and cold ends reached equilibrium. During this
 stable stage, the average temperatures of the hot
 (point A) and cold (point B) ends were measured as
 206.7 and 40.3 °C, respectively.

The temperature data obtained from the TM sam-
 ple were used as original temperature parameter for
 finite-element modeling (FEM). The calculated tem-
 perature distributions in the TM setup and the solder
 seam are presented in Fig. 3. According to the sim-
 ulation results, the temperature of hot side of the
 solder seam reached 181.4 °C, while the temperature
 of the cold side could reach 170.7 °C. In such a case,
 the temperature difference in the solder seam could
 achieve 1070 K/cm, since the width of the solder
 seam was 100 μm; the average environmental tem-
 perature at the solder seam was approximately
 176 °C. According to previous studies [37], TM in
 lead-free solders can be triggered when the temper-
 ature gradient and the environmental temperature
 reach at least 1000 K/cm and 100 °C, respectively. In
 this work, it is clear that the obtained levels of tem-
 perature gradient and environmental temperature in
 the solder seam properly meet these requirements.

Figure 2 Evolution of temperature at points A and B with stressing time.



290 Thus, the TM setup and the produced sample are
291 feasible for the TM tests.

292 Microstructural evolution

293 The microstructures of both plain and composite
294 solder seams after different TM stressing times are
295 shown in Figs. 4 and 5; the variation in thickness of
296 interfacial Sn-Cu IMCs during TM testing is plotted
297 in Fig. 6. It can be found from images of the solder
298 seam before the TM test that β -Sn, Ag_3Sn IMC and
299 Cu_6Sn_5 IMC were present in both kinds of solder
300 seams. It is worth noting that the sizes of β -Sn phase
301 and Ag_3Sn IMCs in the fullerene-reinforced com-
302 posite solder seam were found to be apparently
303 smaller than that in the plain SAC305 solder seam.
304 This phenomenon can be explained in the following
305 way: the added foreign reinforcement provided more
306 nucleation sites during the solidification process; they
307 also could impede the growth of grains by hindering
308 atomic diffusion [35]. With the TM stressing time
309 increasing, large quantities of bulky Cu-Sn IMCs can
310 be found in both plain and composite solder seams;
311 these Cu-Sn IMC are a mixture of the initial Cu_6Sn_5
312 in the SAC305 solder and the newly formed Cu_6Sn_5 as
313 a result of dissolution and migration of Cu atoms
314 coming from the Cu substrates. However, it is
315 apparent that the size and quantity of these Cu-Sn
316 IMCs in the plain SAC305 solder seam were larger
317 than those in the composite solder seam, as shown in
318 Figs. 4d, g, j and 5d, g, j. For the unreinforced SAC305
319 sample, it was found that Cu-Sn IMCs formed first at

the hot end and the central position of the solder
320 seam after 200 h stressing. With the stressing time
321 increasing, the amount of Cu-Sn IMCs continued to
322 grow, and these oval-shaped IMCs were also gradu-
323 ally distributed in the whole solder seam (after 400 h
324 stressing). After 600 h TM stressing, most of the Cu-
325 Sn IMCs were observed to locate at the central position
326 and the cold end of the solder seam. By contrast,
327 after 200 h TM stressing, although the formation and
328 location of Cu-Sn IMCs in the fullerene-reinforced
329 solder seam are similar to those in the plain solder
330 seam, the size of these newly formed IMCs was
331 clearly smaller when compared to their counterparts
332 in the unreinforced SAC305 solder seam after the
333 same stressing time. In addition, there is also a big
334 difference in microstructures for two solder seams
335 after 400 h and 600 h of TM stressing. Specifically,
336 Cu-Sn IMCs formed as result of Cu diffusion were
337 found in both solder seams at the early stressing
338 stage (0–200 h); however, compared to the obvious
339 migration of Cu-Sn IMCs in the plain solder seam,
340 the changes of location of these IMCs in the composite
341 solder seam were not that evident over time. Fur-
342 thermore, most of IMCs in the composite solder seam
343 were still located at the hot end and the central
344 position after 400 h and 600 h stressing; only a small
345 part of these IMCs were found at the position closed
346 to the cold end, since the distribution of reinforce-
347 ment added in the composite solder seam might not
348 relatively uniform after reflow process.
349

In addition to the difference in microstructural
350 evolution for two solder seams, the growth
351

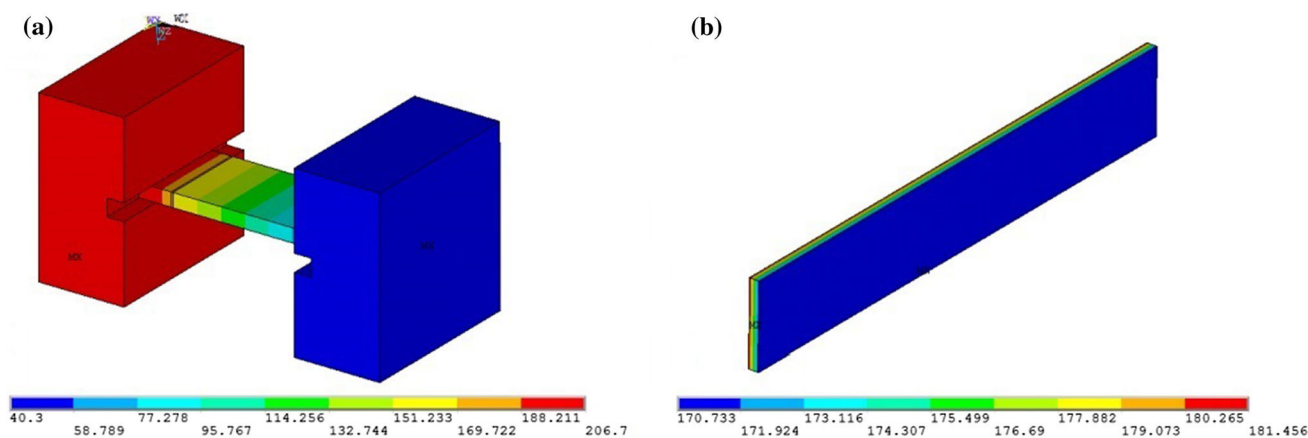


Figure 3 Temperature distributions in TM setup (a) and solder seam (b).

352 characteristics of interfacial IMCs of two types of
 353 samples were also different during TM stressing. For
 354 the plain solder seam, as shown in Fig. 4, the thick-
 355 ness of interfacial IMCs at the cold end obviously
 356 increased with the stressing time. The measured data
 357 for thickness shown in Fig. 6a also confirmed this
 358 trend; the thickness of interfacial IMCs at the cold
 359 end increased from the initial 2.12 μm to 8.96 μm
 360 after 600 h stressing, i.e., approximately 323 %. In
 361 addition, the morphological evolution of interfacial
 362 IMC at hot end also worth noting. It can also be
 363 found from Fig. 4 that the thickness of interfacial
 364 IMCs at the hot end similarly showed a gradually
 365 increasing trend during the first 400 h of stressing;
 366 the thickness increased from 2.51 μm to 3.36 μm , as
 367 shown in Fig. 6a. However, the thickness variation of
 368 interfacial IMC at hot end was not that pronounced
 369 compared to that for the cold end. Further, some
 370 Kirkendall voids were found in interfacial IMCs at
 371 the hot end after 400 h of TM stressing (see Fig. 4i).
 372 After 600 h of stressing, it can be seen that the initial
 373 interface at the hot end was damaged; only a very
 374 thin layer of IMC retained on the Cu substrate. The
 375 interfacial damage at the hot end can be attributed to
 376 considerable diffusion and migration of Cu atoms
 377 from the substrate into the solder seam during the
 378 TM stressing process; this interfacial damage also
 379 further blocked diffusion pathways for Cu atoms. As
 380 to the cold end, some granular Ag_3Sn phase with
 381 light gray color was also observed in Cu_6Sn_5 inter-
 382 facial IMC after 600 h of TM stressing. The observed
 383 formation, migration, and location of Cu-Sn and Sn-
 384 Ag IMCs in the SAC305 solder seam during TM
 385 stressing illuminate that both Cu and Ag atoms

migrate from the hot end to the cold one under the
 large temperature gradient; this finding in the pre-
 sent study is consistent with the current research
 results obtained by other researchers [15, 38].

In contrast, the growth of interfacial IMCs between
 the composite solder seam and the Cu substrates was
 mitigated considerably during TM stressing. Specif-
 ically, the thickness of interfacial IMCs at the cold
 end similarly showed an increase with the stressing
 time, from initial 1.86 to 4.86 μm after 600 h (Fig. 6b).
 The thickness increment for interfacial IMC at the
 cold end was approximately 161 %, significantly less
 than that in the plain SAC305 solder seam. In addi-
 tion, no Ag_3Sn phase was found in interfacial IMCs
 at the cold end after 400 h or 600 h of TM stressing.
 For the hot end, the thickness of interfacial IMCs also
 increased with the stressing time, from initial 2.14 to
 3.52 μm after 600 h. However, in contrast to serious
 damage happened at the hot interface in the plain
 SAC305 solder seam, morphology of interfacial IMCs
 at the hot end in the composite solder seam
 remained intact even after 600 h stressing, except
 that only a few of Kirkendall voids were found in
 this area. Thus, it is believed that incorporation of
 fullerene reinforcement inhibited the dissolution
 process of the Cu substrate, formation, and migration
 of Cu-Sn IMCs as well as the growth of interfacial
 IMCs. Based on the microstructural comparison
 between the plain and composite solder seams after
 TM stressing, the retardation of growth and migra-
 tion of IMCs in the solder seam can be explained as
 follows. Fullerene is a nonreactive, noncoarsening
 material, when appearing in grain boundaries; pre-
 sent fullerene might hinder the migration of atoms

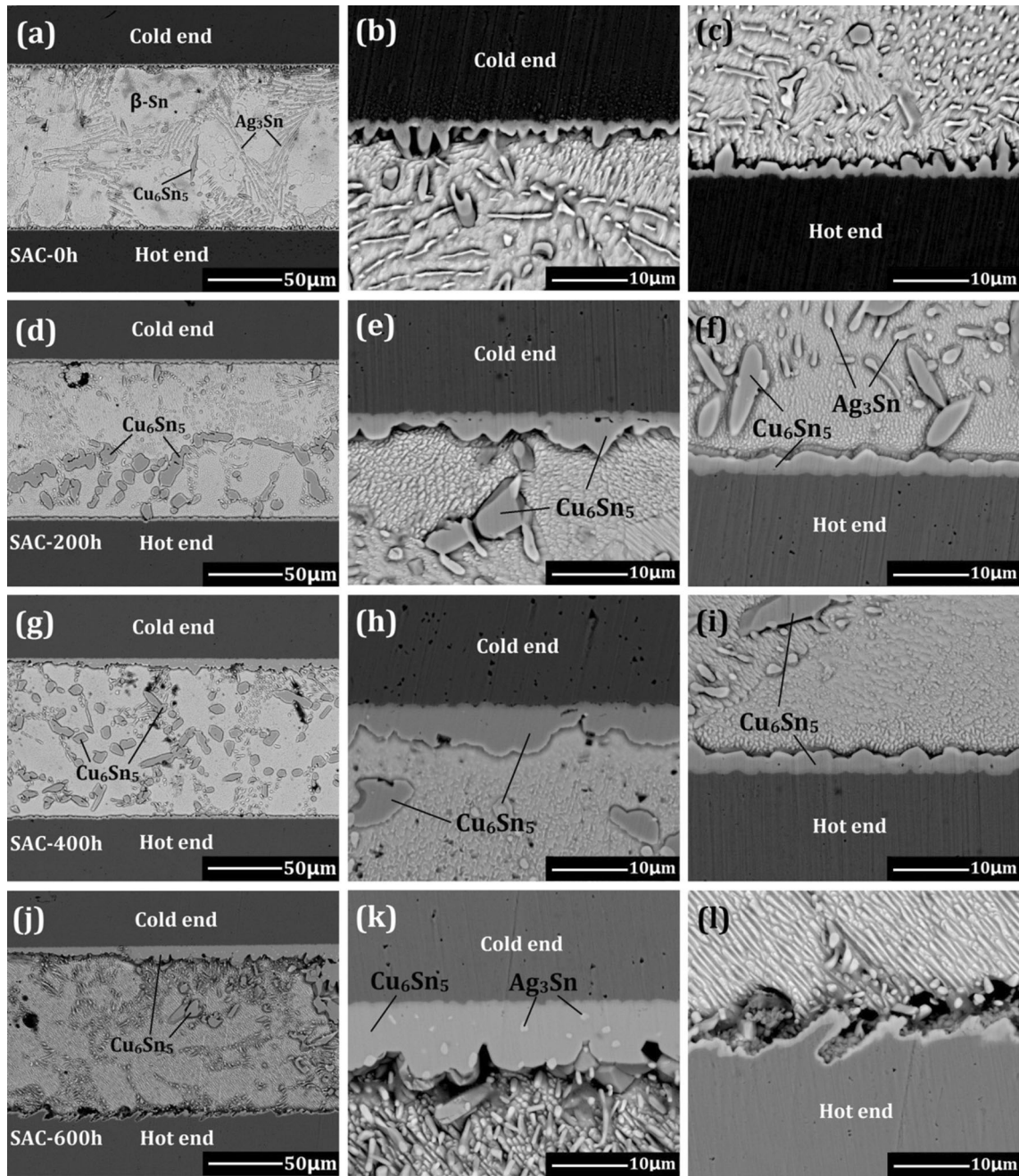


Figure 4 Microstructural evolution of SAC305 solder seam under temperature gradient of 1072 K/cm: **a–c** initial; **d–f** 200 h; **g–i** 400 h; **j–l** 600 h.

420 which could otherwise accelerate the process of IMC
 421 formation. Thus, the relationship between the
 422 growth rates for different crystal orientations of
 423 IMCs changed, leading to restrictions on growth and
 424 migration of IMCs. It is also widely believed that the
 425 diffusion coefficient of Cu atoms in the Sn matrix is
 426 relatively large [39]. Thus, combined diffusion
 427 between Cu and Sn atoms determined the growth of

the interfacial Cu-Sn IMC phase at the solder/copper
 interface. According to our previous study on loca-
 tion of fullerene added in the solder matrix [35], it is
 supposed that some fullerene reinforcement stuck
 around the Cu-Sn phases, acting as barriers for dif-
 fusion of Sn to the Cu substrate or even obstructing
 formation of Cu_6Sn_5 , inhibiting the growth of an
 interfacial IMC layer.

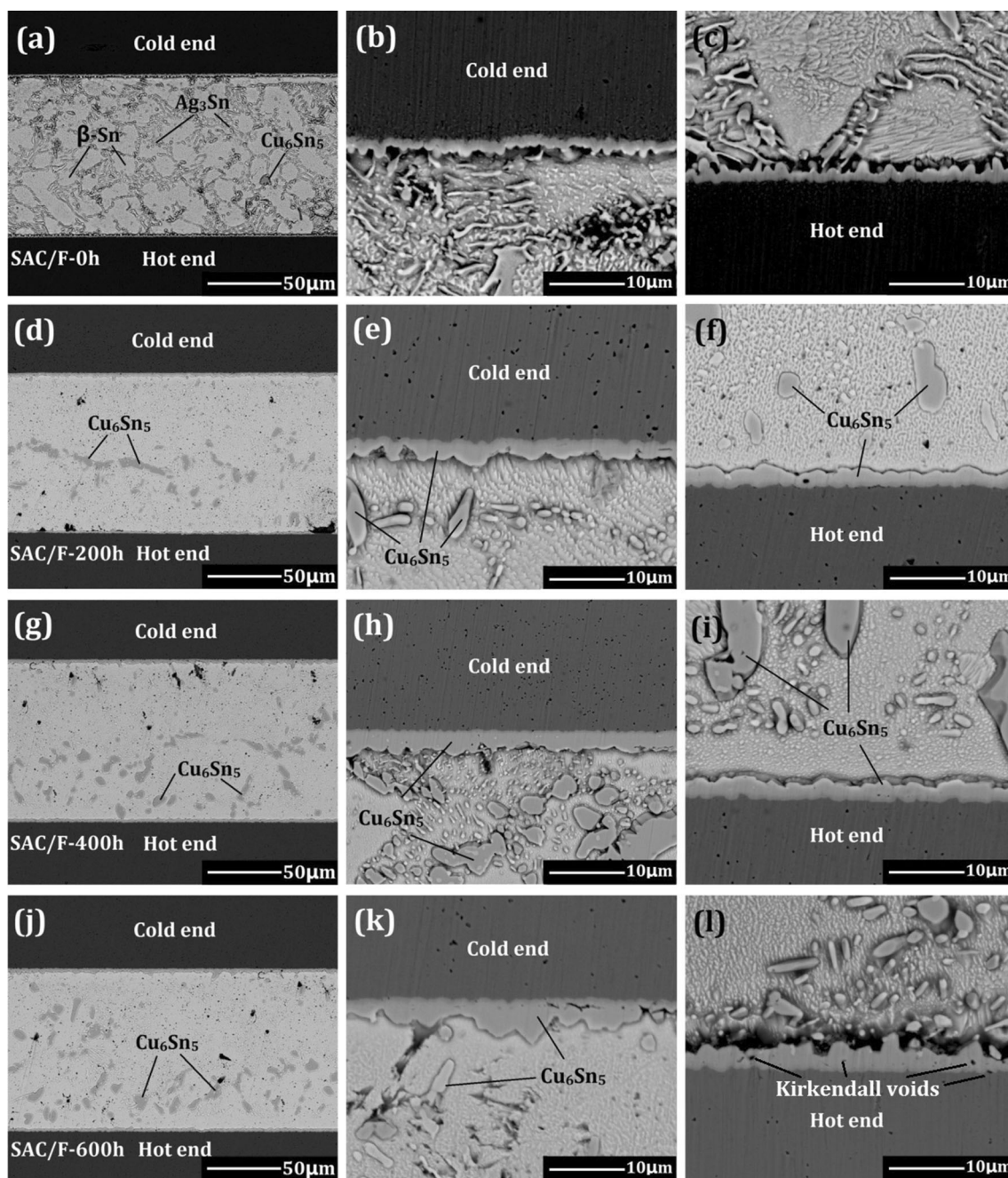


Figure 5 Microstructural evolution of SAC305/F composite solder seam under temperature gradient of 1072 K/cm: **a–c** original; **d–f** 200 h; **g–i** 400 h; **j–l** 600 h.

436 In addition, to understand further the distribution
 437 position of Cu-Sn IMCs in a subsurface layer of the
 438 solder seam, a dovetail groove with depth of 10 μm
 439 was prepared on the solder seams after 600 h of
 440 stressing using FIB, and the respective images are
 441 shown in Fig. 7. It can be known that after a long-
 442 term TM stressing, most of Cu-Sn IMCs formed by

443 Cu diffusion were found to locate at the central
 444 position and the cold end of the plain SAC305 solder
 445 seam; the size and location of these IMCs were con-
 446 sistent with the SEM results as shown in Fig. 4.
 447 Similarly, the observed location and size of Cu-Sn
 448 IMCs in the composite solder seam using FIB were
 449 almost the same as the results shown in Fig. 5. The

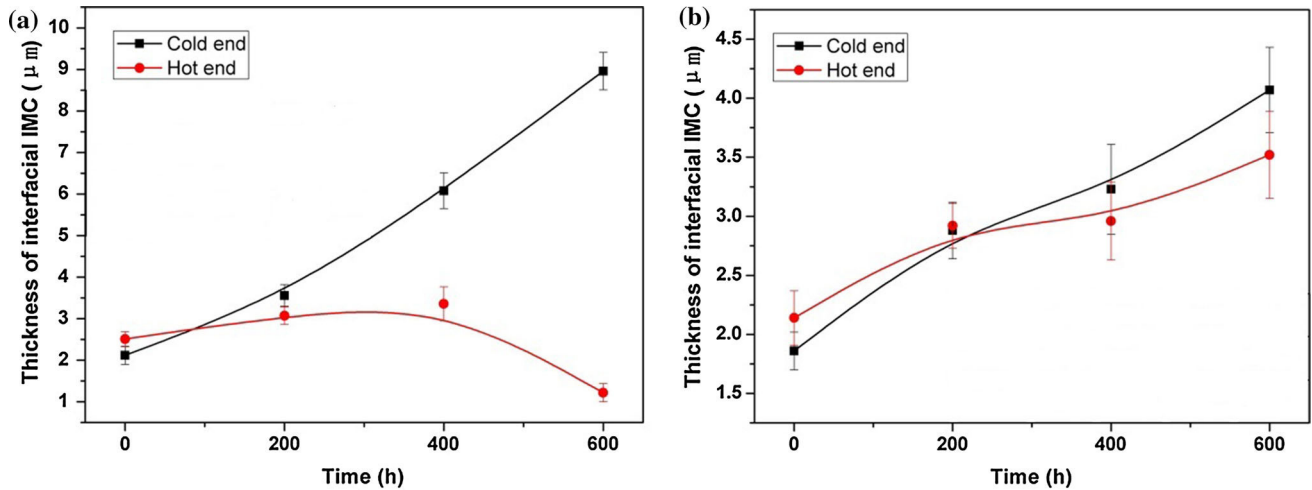


Figure 6 Evolution of thickness of Cu-Sn IMCs at the Cu/SAC305/Cu (a) and Cu/SAC305-F/Cu (b) with TM stressing time.

450 difference of location of Cu-Sn IMCs in the subsurface layer of two kinds for solder seams further indicates that the presence of foreign reinforcement can not only retard the migration of atoms on surface of the solder seam but also mitigate this diffusion in the inner of the solder seam.

456 To quantitatively measure the effect of addition of fullerene on diffusion of Cu atoms from the Cu substrate to the solder seams, the weight percentages of Cu in the solder seams were analyzed after different TM stressing times using ICP. For the ICP tests, in order to meet the testing requirements (the weight of sample is at least 100 mg) as well as to understand the Cu content as precise as possible, four treated samples (cut and polished solder seams; the weight of each solder seam was approximately 38 mg) were chosen for each kind of solder. The average Cu content for each solder was used as the testing result for comparative analysis; the ICP results are shown in Fig. 8. Although the cutting and polishing processes can cause errors in measuring the content of Cu in the solder seams, the obtained results shown in Fig. 8 revealed an obvious difference in the Cu content in two types of solder seams after different stressing times. Specifically, it increased with the TM stressing time; however, the increase rate in the plain SAC305 solder was much higher than that in the composite solder seam. After 600 h of stressing, the average Cu content in the former reached 4.55 wt %, about 9 times higher than its initial value of 0.52 wt %. In contrast, the average Cu content in the composite solder seam after 600 h stressing was 2.09 wt %; only about 4 times higher

483 than its initial value of 0.51 wt %. It is also worth noting that the increase rate of Cu in the plain SAC305 showed a decreasing trend in the interval from 400 h to 600 h. This phenomenon can also be explained by the fact that the diffusion and migration paths of Cu atoms at the Cu/solder interface were damaged due to a long-term TM stressing; this found change in the Cu content agrees well with the observed results as shown in Fig. 4. To avoid the error caused by the above-described phenomenon, only the data for times below 400 h were used to calculate the dissolution rate of Cu atoms during TM stressing. This rate was calculated employing the following formula:

$$v = \frac{M(w_2 - w_1)}{T}, \quad (1)$$

498 where v is the dissolution rate of Cu atoms, M is the average weight of the solder seam, T is the stressing time, w_1 and w_2 are the weight percentages of Cu in the solder seams after 0 h and 400 h stressing, respectively. After 400 h stressing, the net increase of Cu in the SAC305 solder seam was 3.27 wt %; since the weight of the solder seam was 38 mg, 1.24 mg of Cu was dissolved into the solder seam during 400 h of stressing. Due to the fact that the experimental parameters, including the temperature gradient and environmental temperature within the solder seam were relatively stable, the dissolution rate of Cu atoms from the substrate to the solder seam can thus be calculated as 3.1×10^{-6} g/h. By comparison, the increment of Cu content was only 0.488 mg in the composite solder seam after 400 h stressing; the

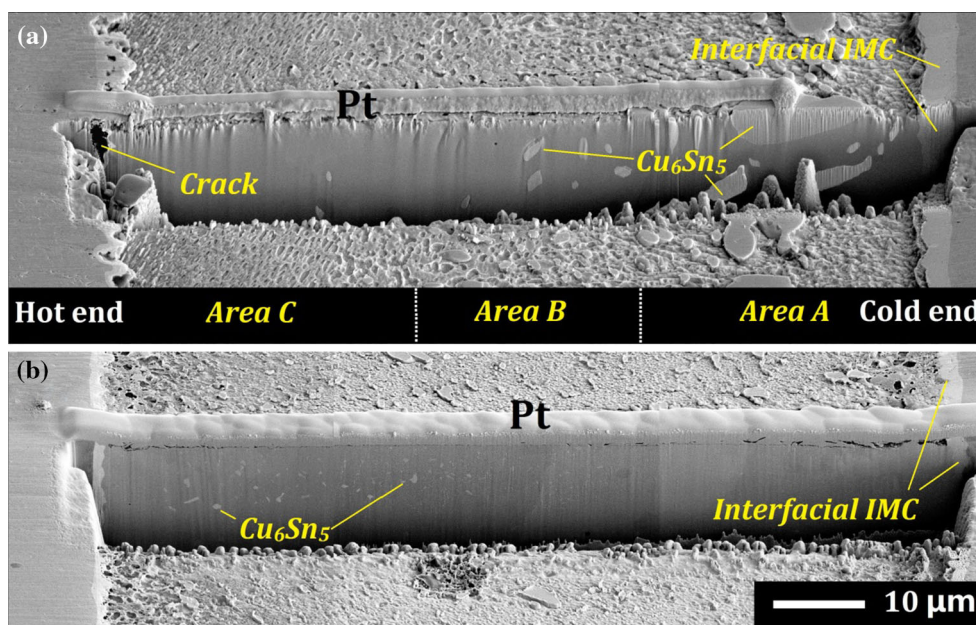


Figure 7 SEM images of FIB-cut trenches on subsurface layer of SAC305 (a) and SAC305/F (b) solder seams.

514 dissolution rate of Cu atoms was calculated as
 515 1.22×10^{-6} g/h, which is only about a half of that in
 516 the plain solder seam. The ICP results and the cal-
 517 culated dissolution rates of Cu atoms clarify that
 518 addition of fullerene reinforcement contributed to
 519 mitigation of the diffusion from the Cu substrate into
 520 the solder seam under TM conditions.

521 To further access the effect of TM on inner struc-
 522 ture of the solder seams, MCT nondestructive scan-
 523 ning was employed to analyze the solder seam area;
 524 the scanning results are shown in Fig. 9. Apparently,
 525 solder seam areas of both types of samples appear
 526 rather intact, without apparent defects before TM
 527 stressing (see Fig. 9a and c). However, big differences
 528 in inner structures were found for two solder seams
 529 after 600 h of TM stressing. Specifically, voids and
 530 cracks caused by elemental migration were found at
 531 both hot and cold interfaces of the plain SAC305
 532 solder seam; further, large amounts of Cu-Sn IMCs
 533 (dark-gray areas) can also be observed at both sides
 534 of the solder seam (Fig. 9b). In contrast, the inner
 535 structure of the composite solder seam after long-
 536 term stressing seems to be less affected when com-
 537 pared with the SAC305 solder seam; only few voids
 538 were found. The newly formed Cu-Sn IMCs (dark-
 539 gray areas) are mainly distributed at the hot side of
 540 the solder seam, while only a small quantity of these
 541 IMCs were found at the cold side (Fig. 9d). The

542 scanning results illustrate that addition of fullerene
 543 reinforcement into solder seam could help to main-
 544 tain this structural integrity, extending the service life
 545 of solder interconnections exposed to a large tem-
 546 perature gradients.

Mechanical properties

547
 548 In most previous studies, hardness of composite
 549 solder joints containing foreign reinforcements was
 550 evaluated using an automatic digital microhardness
 551 tester or a Vickers microhardness tester [11, 40–43].
 552 Some researchers tested hardness and modulus of
 553 solder joints by employing a nanoindenter [44, 45]. By
 554 investigating hardness distribution in solder joints
 555 after current stressing, Ren et al. [46] reported that the
 556 hardness data showed a gradient distribution within
 557 a solder joint from an anode side to a cathode.
 558 However, by now, no studies mentioned the effect of
 559 thermal gradient on mechanical properties of com-
 560 posite solder joints containing foreign reinforcement.
 561 Therefore, in this investigation, to study the
 562 mechanical strength of small areas in solders seams,
 563 nanoindenter was used to assess a variation in
 564 hardness of different solder seams before and after
 565 600 h TM stressing. A constant loading rate of 10 mN
 566 and a dwell time of 5 s were set as the operating
 567 parameters for these tests. Continuous monitoring of

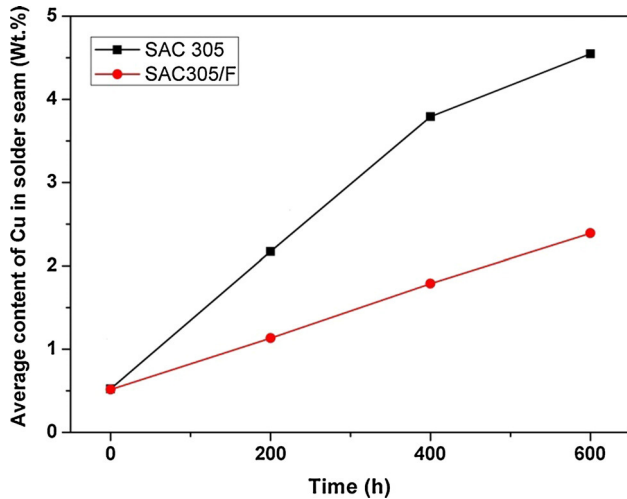


Figure 8 Evolution of weight percentage of Cu in solder seams with stressing time.

568 the constant applied load, constant dwell time, and
 569 indenter's depth displacement was applied to identify
 570 the hardness of different solder seams. In
 571 nanoindentation test, five points were randomly
 572 selected for both plain and composite solder seam
 573 before TM stressing. For the solder seams after 600 h
 574 stressing, as mentioned in the experimental part, five
 575 points were also randomly chosen from A, B, and C
 576 areas for each types of solder seams; the partitioning
 577 of areas A, B, and C is shown in Fig. 7.

578 All load–displacement diagrams for indentation
 579 points and the relevant hardness data for different
 580 samples are shown in Figs. 10 and 11. By comparing
 581 diagrams for the plain and composite solder seams
 582 before stressing, it is clear that the average indenta-
 583 tion depth for the former (1338 nm) is larger than that
 584 for the later (1263 nm). This finding indicates that the
 585 resistance to deformation and hardness of the full-
 586 erene-reinforced composite solder were higher than
 587 those of the plain SAC305 solder. Improved
 588 mechanical strength can be explained as follows. On
 589 the one hand, the reduction in the maximum depth
 590 was due to the decrease in the grain sizes of the plain
 591 solder after doping with 0.1wt. % of fullerene
 592 nanoparticles (see Figs. 4a, 5a). On the other hand, a
 593 dispersion-strengthening effect as well as a pinning
 594 effect caused by introduction of foreign reinforce-
 595 ment also makes a considerable contribution. The
 596 calculated hardness data shown in Table 1 also con-
 597 firms this point of view; the average hardness of the
 598 fullerene-reinforced composite solder seam was
 599 0.256 ± 0.05 GPa, which is 21.9 % higher than that of

0.2562 GPa

the plain SAC solder. However, it was found that a
 scatter in load–displacement diagrams for the com-
 posite solder seam was larger than that for the plain
 solder. This phenomenon indicates that the distribu-
 tion of fullerene in the solder matrix might not be
 homogeneous. As well known, foreign reinforce-
 ment, especially, inert particles (including ceramics
 and carbon-based materials), are hard to be wetted
 reactively by the molten solder; there is a large
 interfacial free energy between the molten solder
 and the reinforcement. Thus, most of the added rein-
 forcement might be excluded out of the molten solder
 during the soldering process, leading to a loss of
 reinforcement and inhomogeneous distributions of
 reinforcement in solder joints. This problem need to
 be further studied in the future to facilitate the
 application of composite solders in the electronic
 industry.

From Fig. 10b and d as well as the hardness data
 shown in Table 1, an obvious difference in indenter
 depths and distributions of hardness data can be
 found for the two studied types of TM stressed solder
 seams. These results vividly demonstrate that the
 hardness data of the plain SAC solder seam after
 600 h stressing gradually decreased from its cold end
 (area A) to the hot end (area C), from the average
 value of 0.2534 GPa for area A to 0.1932 GPa for area
 C. This phenomenon can also be explained using
 migration and redistribution of different elements in
 the solder seam caused by TM stressing. During this
 process, a large amount of Cu atoms dissolved into
 the solder seam, forming Cu–Sn IMCs; these newly
 formed Cu–Sn IMCs were then continually pushed
 toward the cold end by the reverse thrust resulted
 from migration of Sn atoms from the cold end to the
 hot one [15]. In addition, like Cu atoms, Ag atoms
 were also confirmed to move in the same direction
 when the solders were subjected to a large tempera-
 ture gradient. The migration and redistribution of Sn,
 Ag, and Cu during TM stressing would finally lead to
 an increase of Cu–Sn and Ag–Sn IMCs at the cold end
 and the central position of the solder seam. This point
 of view also agrees with the observed results as
 shown in Figs. 4 and 7a. The elemental redistribution
 caused by the temperature gradient would largely
 determine the hardness distribution in the solder
 seams. According to previous reports, the hardness
 values of the β -Sn, Ag_3Sn , and Cu_6Sn_5 phases are
 estimated as 0.35 ± 0.04 GPa [47], 2.9 ± 0.2 GPa [48],
 and 6.10 ± 0.53 GPa [49], respectively. It is apparent

Figure 9 MCT scanning results for plain (a, b) and composite (c, d) solder seams before (a, c) and after (b, d) 600 h stressing.

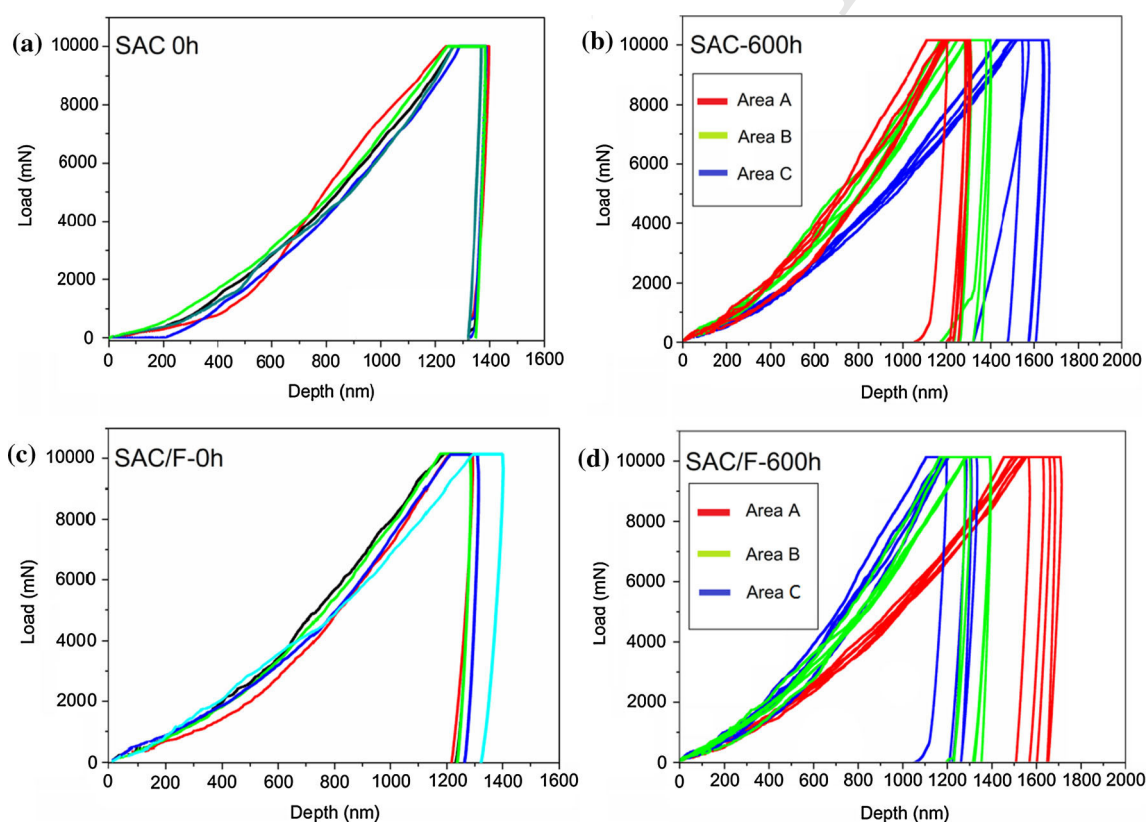
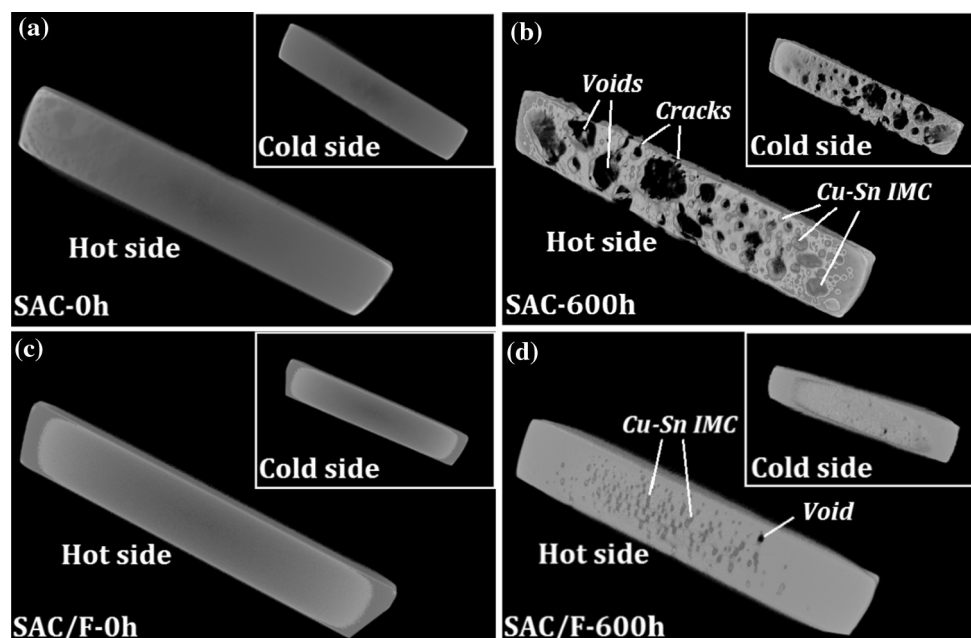


Figure 10 Testing results of indentation points for plain (a, b) and composite (c, d) solder seams before (a, c) and after (b, d) TM for 600 h.

650 that the enrichment of some rigid phase (including
651 Cu-Sn and Ag-Sn IMCs) at the cold end gave a rise to
652 an improvement of hardness in this area.

In contrast, the distribution of hardness values in 653
the composite solder seam showed an opposite 654
result: the hot end (area C) demonstrated a higher 655

Table 1 Calculated hardness data for plain (a) and composite (b) solder seams before and after 600 h TM stressing

	Plain SAC solder (GPa)	Composite solder (GPa)
Reference Hardness (0 h)	0.2102	0.2562
Area A (600 h)	0.2534	0.2026
Area B (600 h)	0.212	0.2544
Area C (600 h)	0.1932	0.2634

656 hardness value than the cold end (area A). In con-
 657 sideration of the migration features of different ele-
 658 ments as well as the obtained results shown in Figs. 5
 659 and 7b, it can be concluded that the migration rate of
 660 all elements in the composite solder seam was
 661 diminished due to the addition of foreign reinforce-
 662 ment. As described in Sect. 3.2, most of the newly
 663 formed Cu-Sn IMCs were located at the central
 664 position and the hot end of the solder seam (namely,
 665 areas C and B); this was also the main reason for
 666 higher hardness values in these areas than in other
 667 areas. As for the cold end, although it was also
 668 exposed to a large temperature gradient during TM
 669 stressing, it was affected more like an isothermal
 670 aging process, since the migration rate of elements
 671 was largely mitigated. During the stressing period,
 672 the decline in hardness resulting from coarsening of
 673 the β -Sn and Ag₃Sn phases might exceed the
 674 enhancement effect caused by enrichment of Cu-Sn
 675 and Ag-Sn IMCs, leading to the overall decrease in
 676 hardness.

677 Conclusions

678 The SAC305/0.1F lead-free composite solder was
 679 produced through the powder metallurgy route. A
 680 temperature difference generator and relevant TM
 681 samples were designed and prepared; the evaluated
 682 temperature gradient in the solder seam in the setup
 683 was 1070 K/cm. After TM stressing, diffusion of Cu
 684 from the substrate to the solder seam was found in
 685 both plain and composite solders; this phenomenon
 686 was particularly prominent in the unreinforced solder
 687 seam. After 600 h of TM stressing, the interface at the
 688 hot end was damaged considerably, while a signifi-
 689 cant increase in the thickness was found in interfacial
 690 IMCs at the cold end. Although interfacial IMCs in the
 691 composite solder seam also showed an increasing
 692 trend during TM stressing, the interfacial structure
 693 remained intact compared with that of the plain solder
 694 seam. According to ICP results, the dissolution rate of
 695 Cu in the plain SAC305 solder under the employed

696 experimental condition was 3.1×10^{-6} g/h; while for
 697 the composite solder, it was only 1.22×10^{-6} g/h. In
 698 addition, the scanning MCT results revealed that
 699 fullerene reinforcement helped to maintain integrity
 700 of the inner structure. The nanoindentation results
 701 demonstrated that hardness of the solder alloy obvi-
 702 ously improved thanks to the doping of fullerene
 703 nanoparticles; moreover, mitigated elemental migra-
 704 tion caused by the presence of the reinforcement could
 705 alter the distribution of hardness values in a solder
 706 seam under TM stressing. The findings of this study
 707 indicate that addition of fullerene could mitigate the
 708 negative effect of TM; hence, composite solders con-
 709 taining foreign reinforcement have a potential for a
 710 use under harsh service conditions.

Acknowledgements

711 The authors acknowledge research funding by the
 712 National Nature Science Foundation of China (NSFC)
 713 and The Research Grants Council (RGC) Joint Research
 714 project (NSFC No. 61261160498, RGC No. CityU101/
 715 12). This research was also supported by the China-
 716 European Union Technology Cooperation Project (No.
 717 1110) as well as the Marie Curie International Research
 718 Staff Exchange Scheme Project within the 7th European
 719 Community Framework Programme, (No. PIRSES-GA-
 720 2010-269113). Thanks are also to the Analytical and
 721 Testing Centre at Huazhong University of Science
 722 Technology as well as LMCC at Loughborough
 723 University for their analytical and testing services.
 724

Compliance with ethical standards

725 **Conflict of Interest** We declare that no conflict of
 726 interest exists in the present manuscript.
 727

References

- 728
 729 [1] Ervina EMN, Amares S, Yap TC (2013) A review: influence
 730 of nanoparticles reinforced on solder alloy. *Solder Surf Mt*
 731 *Tech* 25:229–241

- 732 [2] Hu X, Chen W, Wu B (2012) Microstructure and tensile
733 properties of Sn-1Cu lead-free solder alloy produced by
734 directional solidification. *Mater Sci Eng A* 556:816–823
- 735 [3] Li Y, Moon K, Wong CP (2005) Electronics without lead.
736 *Science* 308:1419–1420
- 737 [4] Basaran C, Abdulhamid MF (2009) Low temperature elec-
738 tromigration and thermomigration in lead-free solder joints.
739 *Mech Mater* 41:1223–1241
- 740 [5] Chen C, Tong HM, Tu KN (2010) Electromigration and
741 thermomigration in Pb-free flip-chip solder joints. *Annu Rev*
742 *Mater Res* 40:531–555
- 743 [6] Ye H, Basaran C, Hopkins D (2003) Thermomigration in Pb-
744 Sn solder joints under joule heating during electric current
745 stressing. *Appl Phys Lett* 82:1045–1047
- 746 [7] Ye H, Basaran C, Hopkins D (2004) Mechanical implica-
747 tions of high current densities in flip chip solder joints. *Int J*
748 *Damage Mech* 13:335–346
- 749 [8] Basaran C, Ye H, Hopkins D, Frear D, Lin JK (2005) Failure
750 modes of flip chip solder joints under high electrical current
751 density. *Trans ASME J Elect Pack* 127:157–163
- 752 [9] Abdulhamid M, Li S, Basaran C (2008) Thermomigration in
753 lead-free solder joints. *Int J Mater Struct Integ* 2:11–34
- 754 [10] Basaran C, Li S, Abdulhamid M (2008) Thermomigration
755 induced degradation in solder alloys. *J Appl Phys*
756 103:123520–123529
- 757 [11] Abdulhamid M, Basaran C (2009) Influence of thermomi-
758 gration on lead-free solder joint mechanical properties. *Trans*
759 *ASME J Electr Pack* 131:011002-1–01100212
- 760 [12] Abdulhamid M, Basaran C, Lai YS (2009) Thermomigration
761 vs. electromigration in microelectronics solder joints. *IEEE*
762 *Trans Adv Packag* 32:627–635
- 763 [13] Ma H (2009) Constitutive models of creep for lead-free
764 solders. *J Mater Sci* 44:3841–3851
- 765 [14] Huang ML, Zhou Q, Zhao N, Liu XY, Zhang ZJ (2014)
766 Reverse polarity effect and cross-solder interaction in Cu/Sn-
767 9Zn/Ni interconnect during liquid-solid electromigration.
768 *J Mater Sci* 49:1755–1763
- 769 [15] Chen C, Hsiao HY, Chang YW, Ouyang FY, Tu KN (2012)
770 Thermomigration in solder joints. *Mater Sci Eng R*
771 73:85–100
- 772 [16] Gao LL, Xue SB, Zhang L, Sheng Z, Ji F, Dai W, Yu SL, Zeng G
773 (2010) Effect of alloying elements on properties and microstruc-
774 tures of Sn-Ag-Cu solders. *Microelectron Eng* 87:2025–2034
- 775 [17] Wang CH, Li KT, Lin CY (2015) Minor Ga addition to
776 effectively inhibit PdSn₄ growth between Sn solder and Pd
777 substrate. *Intermetallics* 67:102–110
- 778 [18] Han YD, Jing HY, Nai SML, Xu LY, Tan CM, Wei J (2012)
779 Interfacial reaction and shear strength of Ni-coated carbon
780 nanotubes reinforced Sn-Ag-Cu solder joints during thermal
781 cycling. *Intermetallics* 31:72–78
- [19] Sobhy M, El-Refai AM, Mousa MM, Saad G (2015) Effect
782 of ageing time on the tensile behavior of Sn-3.5 wt% Ag-0.5
783 wt% Cu (SAC355) solder alloy with and without adding
784 ZnO nanoparticles. *Mater Sci Eng A* 646:82–89 785
- [20] Chellvarajoo S, Abdullah MZ, Samsudin Z (2015) Effects of
786 Fe₂NiO₄ nanoparticles addition into lead free Sn-3.0Ag-
787 0.5Cu solder pastes on microstructure and mechanical
788 properties after reflow soldering process. *Mater Des*
789 67:197–208 790
- [21] Tay SL, Haseeb ASMA, Johan MR, Munroe PR, Quadir MZ
791 (2013) Influence of Ni nanoparticle on the morphology and
792 growth of interfacial intermetallic compounds between
793 Sn_{3.8}Ag_{0.7}Cu lead-free solder and copper substrate.
794 *Intermetallics* 33:8–15 795
- [22] Ma LM, Xu GG, Sun J, Guo F, Wang XT (2011) Effects of
796 co additions on electromigration behaviors in Sn–3.0 Ag–
797 0.5 Cu-based solder joint. *J Mater Sci* 46:4896–4905 798
- [23] Bashir MN, Haseeb ASMA, Rahman AZMS, Fazal MA,
799 Kao CR (2015) Reduction of electromigration damage in
800 SAC305 solder joints by adding Ni nanoparticles through
801 flux doping. *J Mater Sci* 46:6748–6756 802
- [24] He HW, Xu GC, Guo F (2009) Effect of small amount of
803 rare earth addition on electromigration in eutectic SnBi
804 solder reaction couple. *J Mater Sci* 44:2089–2096 805
- [25] Zhao R, Ma LM, Zuo Y, Liu SH, Guo F (2013) Retarding
806 electromigration in lead-free solder joints by alloying and
807 composite approaches. *J Electron Mater* 42:280–287 808
- [26] Hu X, Chan YC, Zhang KL, Yung KC (2013) Effect of
809 graphene doping on microstructural and mechanical prop-
810 erties of Sn–8Zn–3Bi solder joints together with electromi-
811 gration analysis. *J Alloy Compd* 580:162–171 812
- [27] Guo F, Xu G, He H (2009) Electromigration behaviors in Sb
813 particle-reinforced composite eutectic SnAgCu solder joints.
814 *J Mater Sci* 44:5595–5601 815
- [28] Wang FD, Jin C, Liang H, Tang Y, Zhang H, Yang YJ (2014)
816 Effects of fullerene C60 nanoparticles on A549 cells. *Envi-
817 ron Toxicol Phar* 37:656–661 818
- [29] Li H, Tee BCK, Cha JJ, Cui Y, Chung JW, Lee SY, Bao Z
819 (2012) High-mobility field effect transistors from large-area
820 solution-grown aligned C60 single crystals. *J Am Chem Soc*
821 134:2760–2765 822
- [30] John P, Harris F (1999) Carbon nanotubes and related
823 structures. Cambridge University Press, Cambridge 824
- [31] Calvert P (1999) Nanotube composites: a recipe for strength.
825 *Nature* 399:210–211 826
- [32] Komatsu K, Murata M, Murata Y (2005) Encapsulation of
827 molecular hydrogen in fullerene C60 by organic synthesis.
828 *Science* 307:238–240 829
- [33] Chernogorova O, Drozdova E, Ovchinnikova I, Soldatov
830 AV, Ekimov E (2012) Structure and properties of superelastic
831

- 832 hard carbon phase created in fullerene-metal composites by
833 high temperature-high pressure treatment. *J Appl Phys*
834 111:112601–112605
- 835 [34] Watanabe H, Fukusumi M, Ishikawa K, Shimizu T (2006)
836 Superplasticity in a fullerene-dispersed Mg–Al–Zn alloy
837 composite. *Scripta Mater* 54:1575–1580
- 838 [35] Chen G, Wu FS, Liu C, Xia W, Liu H (2015) Effects of
839 fullerenes reinforcement on the performance of 96.5Sn–
840 3Ag–0.5Cu lead-free solder. *Mater Sci Eng A* 636:484–492
- 841 [36] Huang AT, Gusak AM, Tu KN, Lai YS (2006) Thermomi-
842 gration in SnPb composite flip chip solder joints. *Appl Phys*
843 *Lett* 88:141911–141913
- 844 [37] Ouyang FY, Kao CL (2011) In situ observation of ther-
845 momigration of Sn atoms to the hot end of 96.5Sn–3Ag–
846 0.5Cu flip chip solder joints. *J Appl Phys*
847 110:123525–123529
- 848 [38] Huntington HB (1973) In: Aaronson HI (ed) *Diffusion,*
849 *american society for metals.* OH, Metals Park
- 850 [39] Chang CW, Yang SC, Tu CT, Kao CR (2007) Cross-inter-
851 action between Ni and Cu across Sn layers with different
852 thickness. *J Electron Mater* 36:1455–1461
- 853 [40] Tang Y, Li GY, Pan YC (2014) Effects of TiO₂ nanoparticles
854 addition on microstructure, microhardness and tensile prop-
855 erties of Sn–3.0Ag–0.5Cu–xTiO₂ composite solder. *Mater*
856 *Des* 55:574–582
- 857 [41] Gain AK, Chan YC, Yung WKC (2011) Microstructure,
858 thermal analysis and hardness of a Sn–Ag–Cu–1 wt% nano-
859 TiO₂ composite solder on flexible ball grid array substrates.
860 *Microelectron Reliab* 51:975–984
- 861 [42] Ping L, Pei Y, Jim L (2008) Effect of SiC nanoparticle
862 additions on microstructure and microhardness of Sn–Ag–
863 Cu solder alloy. *J Electron Mater* 37:874–879
- [43] Chuang TH, Tsao LC, Chung CH, Chang SY (2012) Evo- 864
lution of Ag₃Sn compounds and microhardness of 865
Sn_{3.5}Ag_{0.5}Cu nano-composite solders during different 866
cooling rate and aging. *Mater Des* 39:475–483 867
- [44] Chellvarajoo S, Abdullah MZ, Khor CY (2015) Effects of 868
diamond nanoparticles reinforcement into lead-free Sn– 869
3.0Ag–0.5Cu solder pastes on microstructure and mechani- 870
cal properties after reflow soldering process. *Mater Des* 871
82:206–215 872
- [45] Yang Z, Zhou W, Wu P (2014) Effects of Ni-coated carbon 873
nanotubes addition on the microstructure and mechanical 874
properties of Sn–Ag–Cu solder alloys. *Mater Sci Eng, A* 875
590:295–300 876
- [46] Ren F, Xu LH, Zhang X, Pang HL, Tu KN (2006) In-Situ 877
Study of the Effect of electromigration on strain evolution 878
and mechanical property change in lead-free solder joints, 879
56th Electronic Components and Technology Conference, 880
San Diego, 2006. pp. 0569–5503 881
- [47] Sadiq M, Lecomte JS, Cherkaoui M (2013) Nanoindentation 882
for measuring individual phase mechanical properties of Sn- 883
Ag–Cu lead-free solders incorporating pileup effects. *Chaotic* 884
Model and Simul 2:335–348 885
- [48] Chromik RR, Vinci RP, Allen SL, Notis MR (2003) 886
Nanoindentation measurements on Cu–Sn and Ag–Sn 887
intermetallics formed in Pb-free solder joints. *J Mater Res* 888
18:2251–2261 889
- [49] Jang GY, Lee JW, Duh JG (2004) The nanoindentation 890
characteristics of Cu₆Sn₅, Cu₃Sn, and Ni₃Sn₄ intermetallic 891
compounds in the solder bump. *J Electron Mater* 892
33:1103–1110 893

UNCORRECTED

Journal : **10853**
Article : **234**



Author Query Form

Please ensure you fill out your response to the queries raised below and return this form along with your corrections

Dear Author

During the process of typesetting your article, the following queries have arisen. Please check your typeset proof carefully against the queries listed below and mark the necessary changes either directly on the proof/online grid or in the 'Author's response' area provided below

Query	Details Required	Author's Response
AQ1	Figure 11 had been cited in the text, but not provided, kindly check and amend the changes.	
AQ2	Please check the edits made in the article title and amend if necessary.	

Author's Response

AQ1: "Fig 11"s were changed to "Table 1", please see line 580 and 593

AQ2: "0.256± 0.05 GPa" was changed to "0.2562 GPa".